Mariner 9 Television Reconnaissance of Mars and Its Satellites: Preliminary Results

Abstract. *At orbit insertion on 14 November 1971 the Martian surface was largely obscured by a dust haze with an extinction optical depth that ranged from near unity in the south polar region to probably greater than 2 over most of the planet. The only features clearly visible were the south polar cap, one dark spot in Nix Olympica, and three dark spots in the Tharsis region. During the third week the atmosphere began to clear and surface visibility improved, but contrasts remained a fraction of their normal value. Each of the dark spots that apparently protrude through most of the dust-filled atmosphere has a crater or crater complex in its center. The craters are rimless and have featureless floors that, in the crater complexes, are at different levels. The largest crater within the southernmost spot is approximately 100 kilometers wide. The craters apparently were formed by subsidence and resemble terrestrial calderas. The south polar cap has a regular margin, suggsting very flat topography. Two craters outside the cap have frost on their floors; an apparent crater rim within the cap is frost free, indicating preferential loss of frost from elevated ground. If this is so then the curvilinear streaks, which were frost covered in 1969 and are now clear of frost, may be low-relief ridges. Closeup pictures of Phobos and Deimos show that Phobos is about 25 ± 5 by 21 ± 1 kilometers and Deimos is about 13.5 ± 2 by 12.0 ± 0.5 kilometers. Both have irregular shapes and are highly cratered, with some craters showing raised rims. The satellites are dark objects with geometric albedos of 0.05.*

The Mariner 9 spacecraft arrived at Mars on 14 November 1971 during a planetwide dust storm of unusual intensity. While forcing the postponement of most geologic and cartographic objectives, the storm has provided an unparalleled opportunity to examine at close range a phenomenon connected with Martian meteorology, topography, depositional and erosional processes, and variable features.

On 22 September Earth-based observers (*1*) recorded that a bright yellow cloud had developed over Noachis, in the midsouthern latitudes of Mars. It spread rapidly over the rest of the planet, and in a little more than 2 weeks the entire visible globe was covered by dust; even the south polar cap had disappeared from view of telescopes. By the fifth week the dust storm had reached its peak, exceeding all previously observed Martian storms in obscuration, areal extent, and duration. Over the next several weeks the atmosphere of Mars showed a gradual clearing, and the south polar cap reappeared. Upon is arrival Mariner 9 found the obscuration still severe.

As Mars rotated in the view of the approaching spacecraft, three preorbital science (POS) sequences of photographs were taken, giving total global coverage of the dust-shrouded planet. Only five distinct features could be seen—the south polar cap and four dark spots (Fig. 1). One of these has been identified as Nix Olympica, and the other three (provisionally labeled North, Middle, and South Spots) have been identified with a group of features that

Table 1. Camera filters. The effective wavelength is for sunlight.

Camera	Filter type	Effective wavelength (μm)
Wide angle	Orange	0.610
Wide angle	Green	0.545
Wide angle	Blue	0.477
Wide angle	Violet	0.414
Wide angle	Polarization*	0.565
Wide angle	Yellow (minus blue)	0.560
Narrow angle	Yellow (minus blue)	0.558

* Three filters with axes spaced in 120° steps.

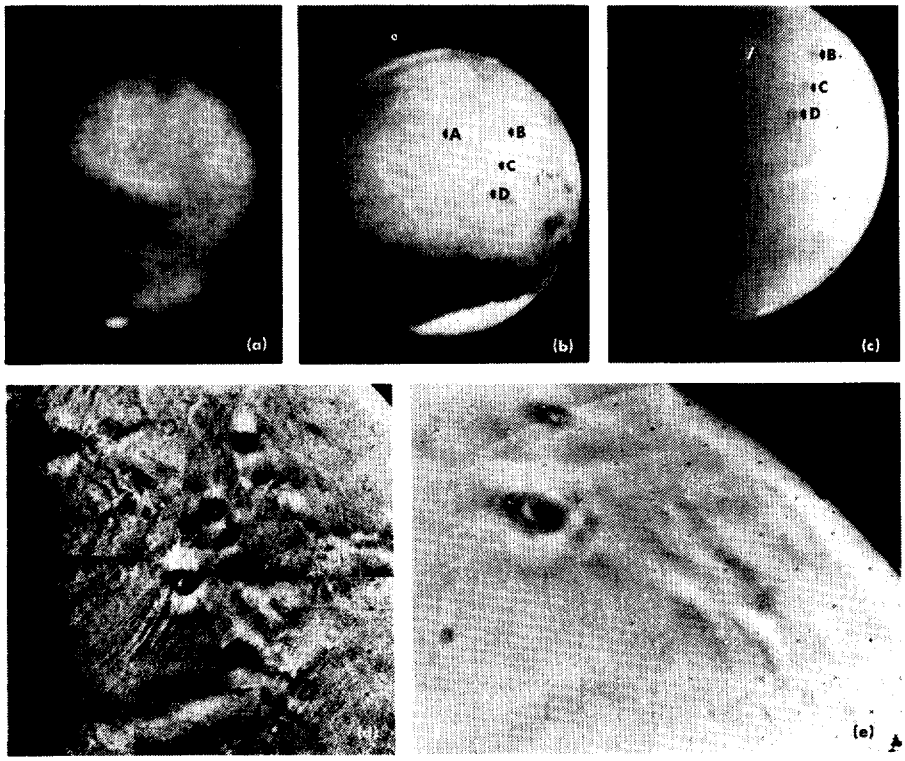

Fig. 1. (a) Telescopic photograph of Mars taken from the earth by E. C. Slipher during the 1956 dust storm (*22*). The dark spot at the top is an example of several such temporary features observed when the planetary surface has been largely obscured by dust. (b) Computer-enhanced picture of Mars taken by Mariner 7 in 1969 (photograph number 7F74). (*A*) Nix Olympica with its ringed appearance and (*B, C, D*) three aligned craterlike features that make up part of the "W-cloud" complex are shown. (c) Slightly enhanced picture of the same region taken by Mariner 9 during POS 2 about 1½ days before insertion (Image Processing Laboratory roll 147, 113230). The small south polar cap shows at the bottom of the planet's disk. A dark spot identified with Nix Olympica and three aligned dark spots that lie on the western part of the "W-cloud" complex are visible. The very low contrast is due to obscuration by the planetwide dust cloud. (d) Filtered mosaic of the four dark spots, taken 1 day later; the streaks run 1000 km south of South Spot (Jet Propulsion Laboratory P-12676). The bright wings on either side of each dark spot are artifacts of the filtering. (e) Filtered picture of South Spot, taken on Rev 24 about 13 days later than (d); the streaks extending south of South Spot are no longer visible (IPL roll 909, 123836). The streaks reappeared in subsequent photographs.

become bright (the "W-cloud") (*2*) during the Martian afternoon at certain seasons. The rest of Mars was veiled by heavy, but regionally variable, atmospheric dust, and it was apparent that Mars was not the same planet for which this mission had been planned.

Gradual clearing began during the third week of orbital operations. The degree of obscuration varies from region to region. The south polar region, for example, has consistently been clearer than other parts of the planet. However, as of this writing (mid-December), Mars is still heavily obscured.

The dust storm has had a pronounced effect on the original mission plan (*3*), which included both global surveillance of Mars and contiguous high-resolution mapping sequences near periapsis. The mapping sequences were soon found to be ineffective: Dust obscuration varied widely, but the mapping sequences could not be made sufficiently flexible to take advantage of the relative clarity of some regions. Also, periapsis was located close to the evening terminator, where the more diffuse illumination at the surface severely degrades surface contrast. It was necessary to direct the high-resolution photography to the few places where it would be effective. Therefore, a new mission plan, the "reconnaissance mode," was developed and implemented on revolution (Rev) 26, the earliest opportunity. This mode included on each revolution, global coverage, from which specific targets in relatively clear areas could be located, and two groups of four high-resolution frames each (tetrads), which could be placed on such targets.

The Mariner 9 spacecraft is equipped with two television cameras (*3*), similar to those flown on Mariners 6 and 7. The wide-angle camera has a field of

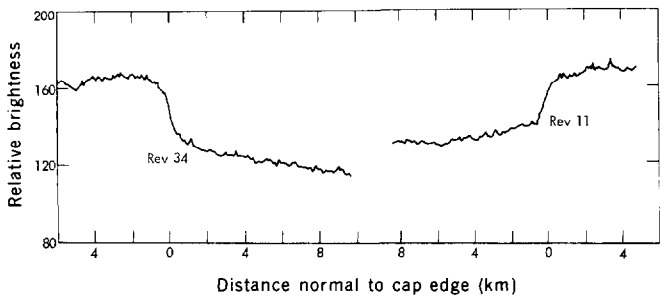

Fig. 2 (left). Profiles of relative brightness across the edge of the polar cap, measured with the narrow-angle camera (yellow filter). The relatively sharp rise represents the discontinuity at the edge of the polar cap. Th gradual decrease in brightness on either side of the edge results from light scattering in the dust above the polar area.

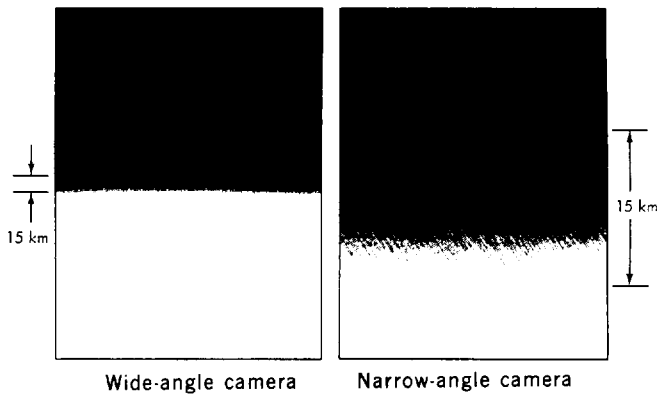

Fig. 3 (right). Photographs of the limb of Mars taken on Rev 16. The view on the left (JPL 4024-13) was taken with the wide-angle camera and a violet filter; that on the right (JPL 4024-10) was taken with the narrow-angle camera and a yellow filter. Note the detached layer of haze about 15 km above the apparent limb of the planet. The limb region is located at 20°S latitude and 102°W longitude.

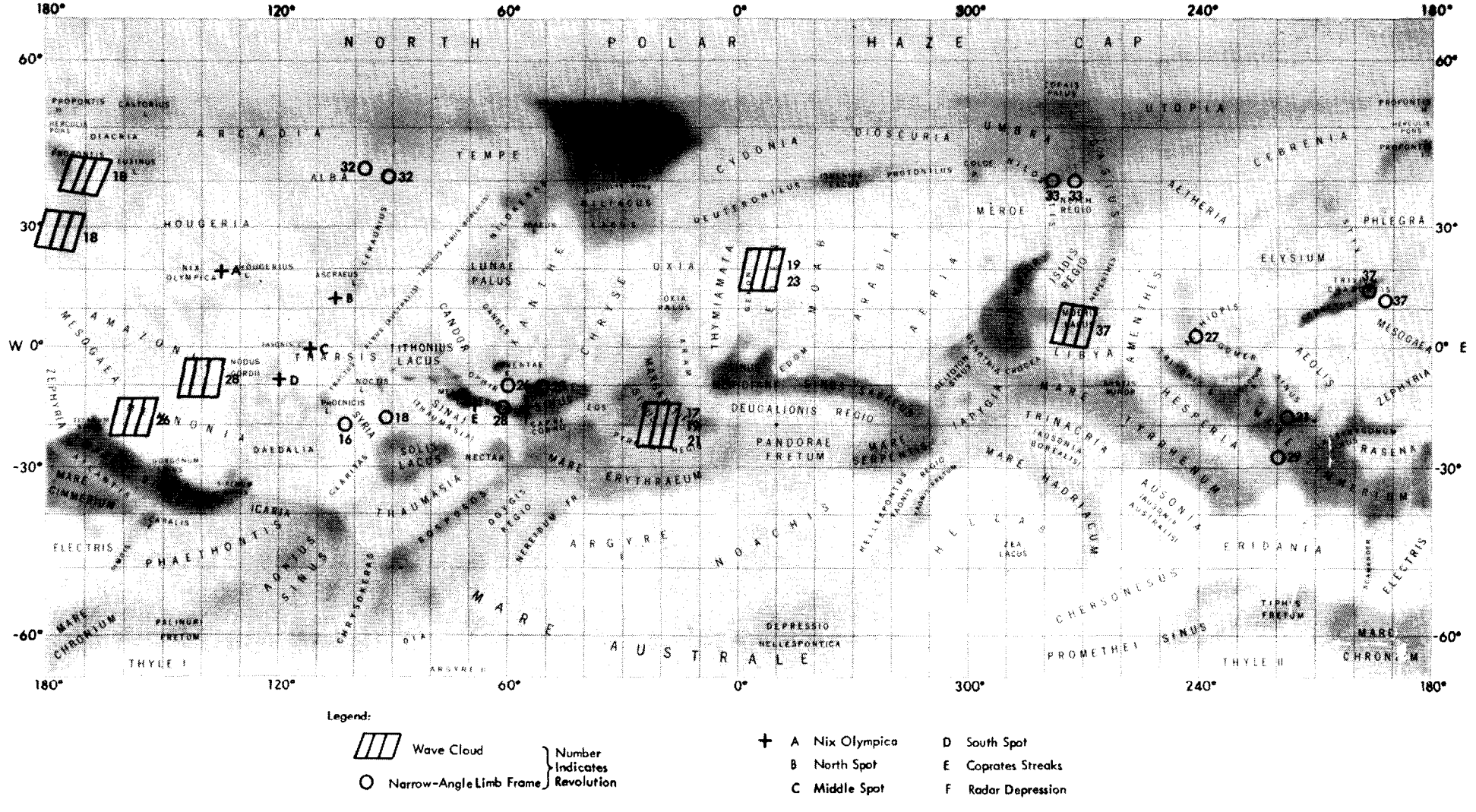

Fig. 4. Mercator map showing the approximate locations of wave clouds visible in violet and blue frames taken with the wide-angle camera. The lines show the orientation of the wave bands. The circles show the positions of narrow-angle frames of the limb. The numbers near the lines and circles designate the revolutions on which the observations were made. The areographic features, Nix Olympica (*A*), the three dark spots (*B, C, D*), the bright streaks in the Eos-Ophir region (*E*), and the radar depression near Eos (*F*), were observed in Mariner 9 photographs.

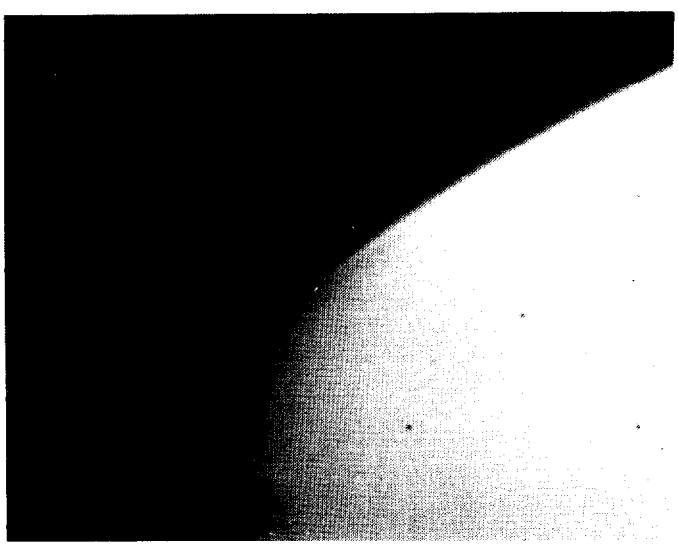

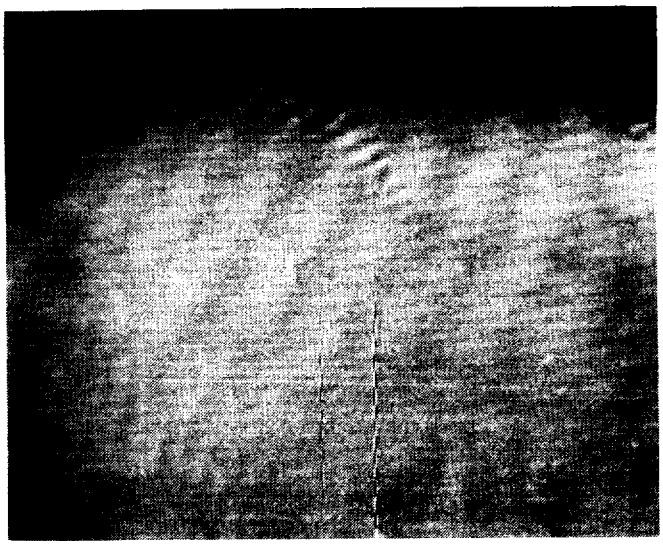

Fig. 5 (left). Detached layer of haze located near the terminator on Rev 29 is about 30°N latitude, 140°W longitude. The thin layer is about 30 km above the extrapolated apparent limb. The picture was taken with the wide-angle camera and violet filter (JPL 4039-19). Fig. 6 (right). Terminator wave clouds in violet wide-angle frame on Rev 18 (IPL roll 813, 164208). The wave crests are approximately parallel to the terminator, and the wavelength is about 40 km. The locations of the waves are shown in Fig. 4.

view of 11° by 14° and employs eight interchangeable filters (Table 1). The narrow-angle camera has a field of view of 1.1° by 1.4° and is equipped with a fixed yellow filter. Thirty-one pictures are taken on each revolution of 12 hours.

Caution must be used in interpreting the details visible in the pictures accompanying this report. Ordinarily, the contrast of visible detail on Mars is some tens of percent. However, the 1971 dust storm has drastically reduced contrasts. In order to make visible any detail other than the polar cap and the four dark spots, it has been necessary to increase the contrast of the Mariner 9 pictures by much more than the usual photographic factor of 2 or 3.

Some of the pictures reproduced here (for example, Figs. 12c and 13) have been photometrically "stretched" so that a small brightness range (usually about 20 percent of the original range of the data) is expanded to cover the full range from white to black. This technique (*4*) is limited by the strong limb-to-terminator brightness gradient (see Fig. 1c). It is not practical to increase the contrast more without first removing the average brightness gradients across a picture. This is accomplished by subtracting a running mean (for example, 175 consecutive picture elements or samples along each line) from the signal level at each sample in the original data. Thus, features much larger than 175 samples in width are removed from the data. The remaining small-detail modulation, typically of the order of a few percent, can then be expanded to cover the full range from white to black. In this way, the contrast of small detail can be increased by a factor of about 50. The process amounts to high-(spatial)-frequency filtering followed by severe "stretching"; for brevity, we call the products "filtered."

It is essential to bear in mind the enormous exaggeration of contrast in such filtered pictures. Most of the detail in the Mariner 9 pictures actually has an order of magnitude less contrast than the weakest telescopic details seen on Mars from the earth. Some examples may help in understanding this contrast exaggeration and certain artifacts.

1) Most of the filtered pictures show a prominent pattern of diffuse vertical stripes, caused by electronic noise on the spacecraft (for example, Fig. 11). The peak-to-peak amplitude of this noise is typically a few tenths of 1 percent, but it is easily visible because it has been amplified some tens of times.

2) Reseau fiducial marks on the vidicon are about three samples across and are almost black. When a reseau falls within the range of a running mean, it lowers the mean by about 2 percent. When this lowered mean is subtracted from a sample near the reseau, the sample appears to be about 2 percent brighter than the mean. Thus, on filtered pictures, each reseau is flanked by two bright lines (of combined length equal to the length of the running

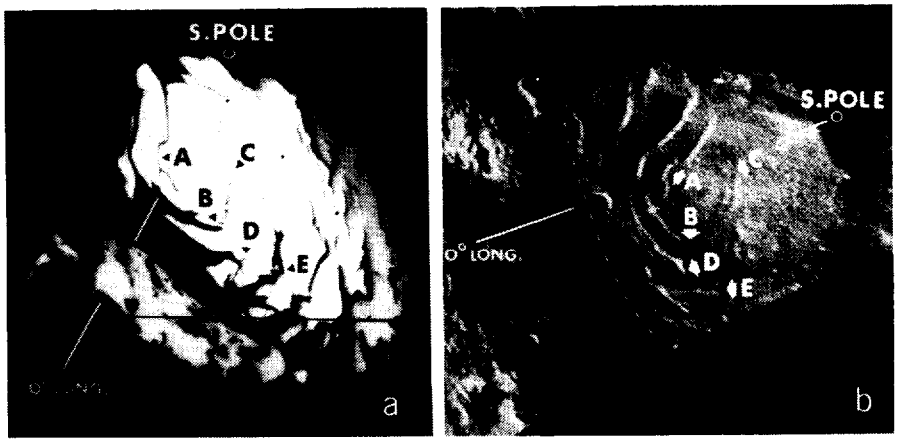

Fig. 7. (a) Mariner 9 (JPL 4019-25) and (b) Mariner 7 (7N17) views of the south polar cap. The dark markings in the Mariner 9 wide-angle view of cap are correlated with the light markings in the Mariner 7 narrow-angle frame. The Mariner 7 image has been rectified and then enhanced. Although (b) shows strong contrast, the entire area actually was covered by frost.

mean) about 2 percent brighter than its surroundings. In most prints these bright lines are almost at the white level (for example, see Fig. 11).

3) Both wide- and narrow-angle pictures show small circular blemishes, about 40 samples in diameter, which are the penumbral shadows of small dust specks on the vidicon faceplates. The contrast of the most prominent shadow is 5 percent in the wide-angle camera and 0.5 percent in the narrow-angle camera. These shadows are invisible on the raw pictures. (In filtered wide-angle pictures, such as Figs. 11 and 12e, they sometimes appear black.)

4) A prominent feature of many pictures is a residual image of an earlier limb picture (see Fig. 12c). This residual is about 10 percent in brightness in the first picture after the limb frame and decays slowly; it is about 5 percent on the next frame, 3 percent on the next, and so on (continuing greater than 1 percent for many frames). For example, the wide-angle pictures from Rev 2 showed prominent limb residuals from the last preorbital sequence. These residuals have about 1 percent peak contrast.

In many processed photographs these artifacts—the streaks about the reseaus, the shadows of the dust specks, the limb residuals, or even the vertical noise—are more prominent than the images of real features on Mars, which shows that the contrast in the scene is less than that of the artifacts. Features of such low contrast would be invisible by telescope or on conventional photographs of Mars.

Photometric function. The limb darkening of the planet is evident in preorbital data. If we assume that the limb darkening can be described by a Minnaert function (*5*, *6*), the darkening parameter k is uniquely related to the position on the disk of maximum brightness, if it is assumed that the view is orthographic (constant phase angle over the disk). This assumption is not quite met, but the angle subtended by the planet is less than 3° in the pictures taken with the wide-angle camera just before orbit insertion. These pictures cover the full range of color filters in quick succession, the maximum value of k occurs on the terminator side of the subsolar point for orange, yellow, and green light, and on the limb side for blue and violet. The corresponding values of k progress regularly from 1.12 to 0.93 with decreasing wavelength, for an assumed mean phase angle of 58°. The differences from a Lambertian surface ($k = 1.00$) are small but significant; the limb is clearly bluer than the center of the disk.

Since the surface features are generally hidden by the dust storm, the quasi-Lambertian limb darkening is not surprising, although data from Mariner 4 (*5*) indicate much lower values of k (0.7 to 0.8). Lambertian surfaces can be approximated in the laboratory by powdered materials of low refractive index that produce high-order multiple scattering. Thus, the present values of k near unity are consonant with an optically thick scattering atmosphere. Unlike the isophotes of a quasi-Lambertian sphere, which are ellipses centered on the subsolar point, the Martian isophotes are elongated toward the poles—consistent with a significant contribution from single scattering. Because the single scattering is nonconservative, it represents an important fraction of the net albedo from multiple scattering. The weak absorption in the scattering is consistent with the scattering material being dust raised from the surface.

Visibility of surface features. The most prominent features in the POS pictures are the south polar cap and the four dark spots. The dark appearance of these spots is particularly striking, as they are usually observed to be at least as bright as their surroundings. However, a dark feature of relatively high contrast, which may have been South Spot, was reported during the 1924 dust storm (*7*), and other temporary dark spots have been noted when the surface of Mars has been obscured

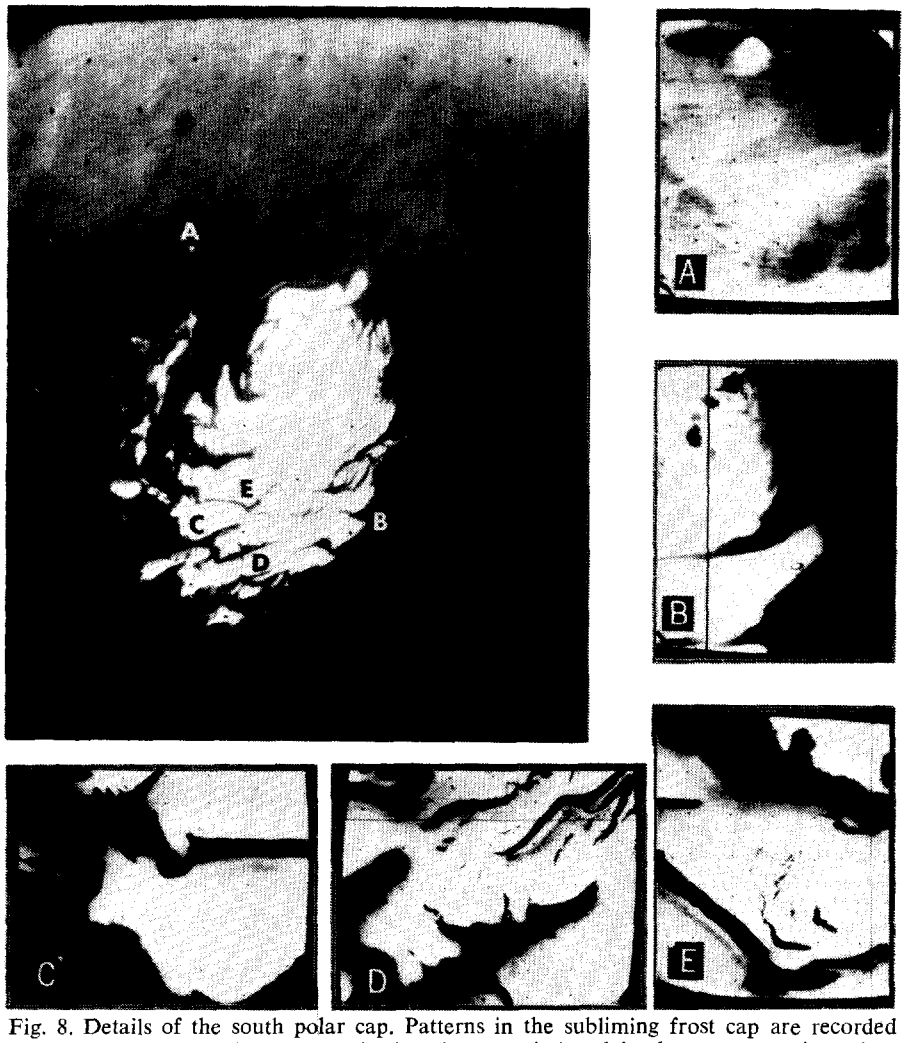

Fig. 8. Details of the south polar cap. Patterns in the subliming frost cap are recorded in the five narrow-angle frames. The locations are indexed in the accompanying wide-angle frame. The maximum dimension of the narrow-angle frames is about 100 km on the surface of Mars. Frames A (JPL 4056-65) and E (JPL 4056-62) are from Rev 46, C (JPL 4045-71) and D (JPL 4048-65) from Rev 38, and B (JPL 4033-45) from Rev 25. The wide-angle frame (JPL 4056-65) is from Rev 46; a residual image of the polar cap is faintly visible, displaced toward the upper right corner.

by dust (Fig. 1a). The maximum contrast (*8*) of the spots was 20 percent for Nix Olympica and 10 percent for South Spot, from Mariner 9. The contrast of the three aligned spots decreased as they rotated toward the early afternoon limb, but Nix Olympica lost contrast toward the limb on only one of the two POS sequences. This behavior suggests that the extinction optical depth τ (*9*) above the three aligned spots was about 1, but it may have been significantly less over Nix Olympica.

Because the south polar cap showed the highest contrast of any surface feature, and because it was observed frequently, it was a useful target for measuring variations in atmospheric extinction. It does not exhibit diurnal brightening as the spots sometimes do. Figure 2 shows typical profiles of relative brightness across the edge of the cap, from narrow-angle frames. The shape of these profiles—a sharp jump in brightness with gradually decreasing variations on each side of the jump—may be due to a sharp-edged cap that appears somewhat diffuse because of atmospheric scattering of the radiation reflected from both sides of the surface albedo boundary (*10*). An alternative interpretation of the features of these brightness profiles, in terms of gradual variations in the intrinsic surface albedo on both sides of the cap edge, seems less likely. With the model of a sharp-edged cap, we derive a contrast of 14 percent at the cap edge on Rev 11. The normal contrast of the cap edge in yellow light is about 90 percent (*11*). The contrast reduction of the Rev 11 narrow-angle picture suggests that τ was about 1, reduced to the zenith, over the cap at that time. The contrast of the cap showed little variation during the first 2 weeks of the mission but began to increase during the third week. By Rev 34 a narrow-angle picture showed significantly more contrast than the Rev 11 frame, and continued contrast increases have been observed on later revolutions. Evidently, τ decreased significantly during this time.

Nix Olympica, the three spots, and the south polar cap were the clearest regions on the planet; other albedo features of large size also were faintly visible, mainly in the southern hemisphere. However, the disappearance of almost all of the classical albedo features and of many craters suggests that τ was 2 or more over most of the planet. Craters, appearing as features of high albedo, can be seen in many pictures taken at high angles of the sun. In general, craters and other albedo features were observed better in orange light than in violet. Some relatively low areas also appear bright, for example, the long, bright streaks in the regions of Ophir and Eos (Fig. 12).

Except in Nix Olympica and the dark spots, surface relief (in contrast to albedo variations) could not be seen during the first 2 weeks. This can be attributed in part to very strong diffusion of solar radiation by the haze, so that surface illumination was nearly isotropic. During the third week, surface relief could be seen more readily, especially near the south polar cap. This observation supports our conclusion from the contrast data for the polar cap that the optical thickness of the haze was diminishing during this period.

Structure of the limb. Figure 3 shows typical limb structure in overlapping narrow- and wide-angle frames. The features shown—a gradual decline in brightness at the limb, a well-defined gap, and a thin elevated layer of haze—were observed in most frames of the apparent limb, with typical scales of 10 km for the region of brightness decline and 15 km for the gap between the limb and the elevated layer. The first dimension suggests that the scattering particles responsible for the decline in brightness are distributed with the scale height of 10 km. The narrow-angle pictures taken north of 15°N showed more complex structure, often with several layers and with horizontal variations in the layers, but all the narrow-angle frames of the limb showed some detached layer structure. The locations of these pictures through Rev 35 are shown in Fig. 4. In addition, four narrow-angle frames showing limb structure were taken south of 65°S. The detached layer shown in Fig. 3 is brighter in the violet wide-angle frame than in the yellow narrow-angle frame, in contrast to the region of brightness decline, which is distinctly brighter in the yellow frame. A photometric four-color sequence including the limb near the south polar cap showed that the planet and the regions of brightness decline were about as red as the normal Mars, which, together with the scale of 10 km, suggests that the lower scatterers are dust particles. The elevated haze was white or slightly blue and is evidently composed of different particles, possibly condensates. Elevated thin layers of haze were also visible at, or just

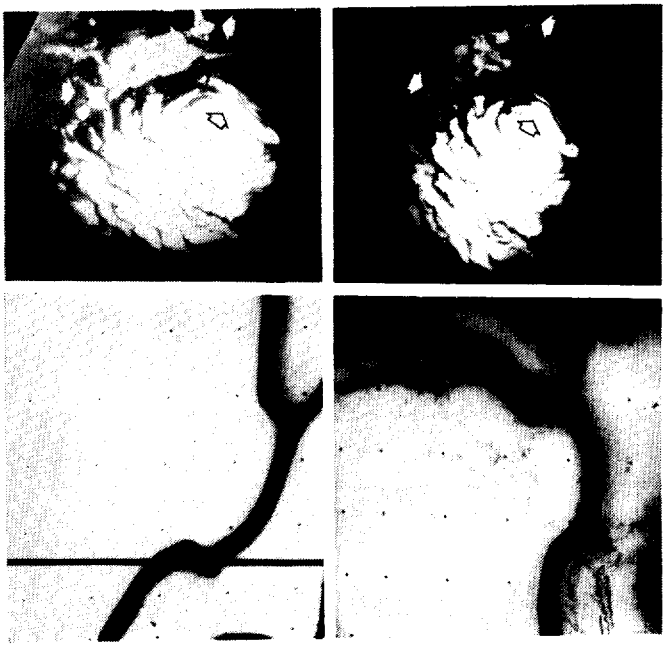

Fig. 9. Mariner 9 photographs displaying the gradual disappearance of the residual polar cap. At the top are two Mariner 9 wide-angle pictures of the polar cap acquired about 9 days apart on Revs 11 (left) and 29 (right). These two images have been rectified to a polar stereographic projection. The relative distortion between the two projections is due to uncertainties in the preliminary pointing data. The cap is approximately 450 km in diameter in the earlier image. The white arrows indicate common areas that have suffered significant defrosting over the 9-day period. A residual image of the cap can be seen to its right in the left-hand picture. At the bottom are two Mariner 9 narrow-angle frames from Revs 11 (left) and 34 (right); these show changes in the cap over 11½ days. The area of the narrow-angle frames is indicated by black arrows in wide-angle frames. Since certain fine details can be seen in both images, the difference in the appearance is real and not solely the result of varying obscuration. Detailed patterns parallel to the main frost-free corridor are emerging in the later version.

beyond, the terminator on the limb (Fig. 5).

Atmospheric waves. Figure 6 shows apparent atmospheric wave structure near the terminator just east of Elysium. Several large wave trains have been seen on the terminator in pictures through Rev 50. Typical wavelengths are 40 km. These features are plotted in Fig. 4. Waves were observed in one wide-angle frame taken with a blue filter; in all other cases they were seen in violet light. None was apparent in orange frames, even when the overlapping violet frames showed waves in the same region on successive days. The brightness variation across a given wave and the increasing contrast near the terminator (Fig. 6) suggest relief variations in an atmospheric scattering layer, but the waves also could be made visible by variations in the optical properties of the scattering layer. Their visibility in violet but not in orange, together with the crisp detail, suggests that these waves are not seen in the top of the main atmospheric dust layer but most likely occur in a higher, bluer layer, possibly of condensates. The occurrence of thin, bright clouds near the terminator (Fig. 5) supports this interpretation. The preferred orientation of the wave crests, parallel to the terminator, is apparently real.

Shorter waves (5 km long) were observed in a few narrow-angle frames (yellow filter), mainly near the terminator. Some features suggestive of waves were also observed in POS narrow-angle frames. The curvilinear streaks that extend nearly 1000 km southwest from South Spot were seen only at low angles of the sun (see Fig. 1, b–d). During a 90-minute period in POS 3 these features exhibited large changes. They may be atmospheric waves in the upper part of the dust layer, controlled by the elevated topography known from Earth-based radar (*12*) to lie to the east. The wave structure seen in the yellow frames is evidence for some vertical structure in the dust, at least locally.

Interpretations. The three aligned dark spots are located at or near points that are high in Earth-based radar profiles. Crater floors are seen as brighter objects than their relatively higher surroundings, although no widespread correlation between craters and higher albedos was noted in the 1969 data (*13*). The long depressions in the Ophir-Melas Lacus region are brighter than their rims. Thus, certain elevated regions (*12*) are relatively dark, and certain regions that are lower than their surroundings appear bright. The apparent connection between bright and dark areas and elevation differences during this dust storm raises the possibility that some classical seasonal and secular variations of features have been due to differential obscuration of areas at different elevations (*14*). In addition, local dust storms could produce local obscuration (*15*), even when no global dust storm is in evidence.

The consistently better visibility of the high areas may be due to concentration of the dust in widespread low layers through which the high terrain protrudes, or to there being less atmo-

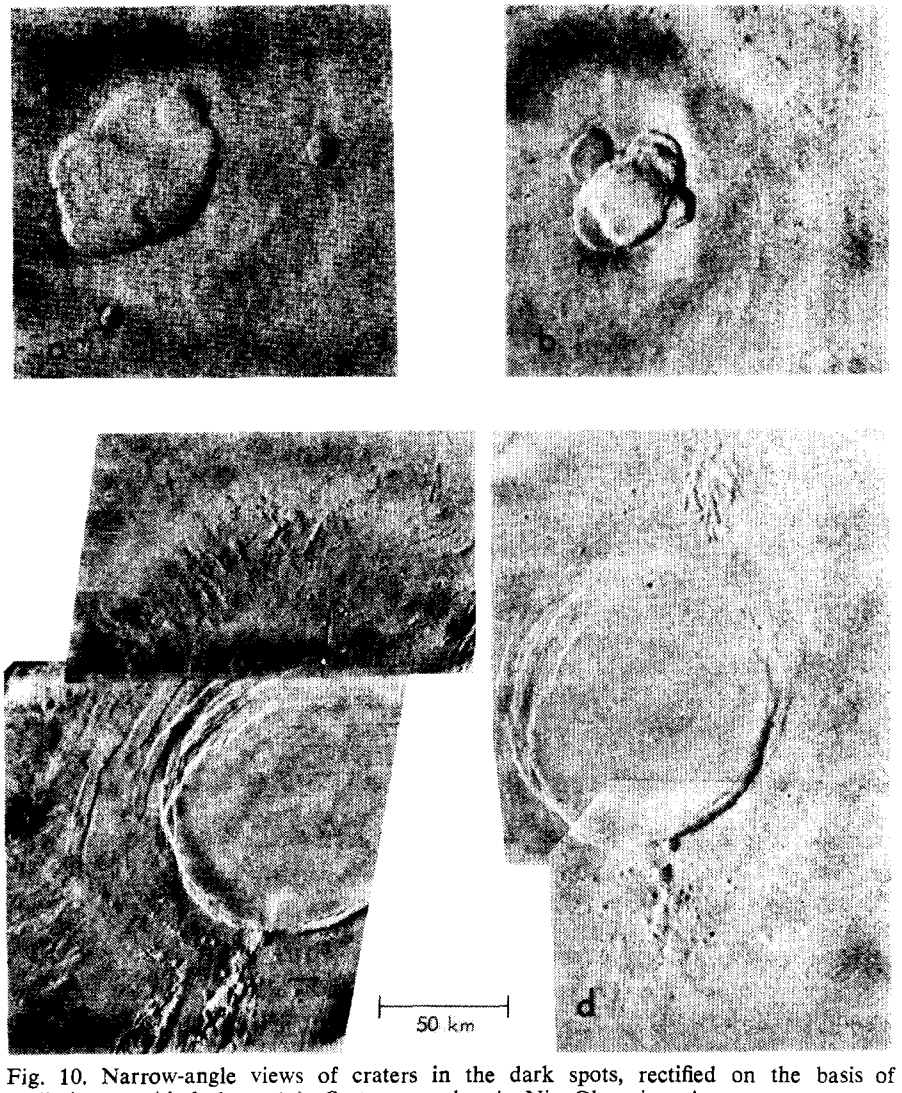

Fig. 10. Narrow-angle views of craters in the dark spots, rectified on the basis of preliminary orbital data. (a) Crater complex in Nix Olympica. Arcuate scarps continuous with the scallops on the wall indicate that the floor is not fully obscured. Smaller craters to the east and south may be superposed, unrelated features (IPL roll 882, 025127). (b) Crater complex of North Spot. The central crater with terraced walls apparently truncates several subsidiary craters (IPL roll 882, 030159). (c) The South Spot crater photographed on Rev 28 (IPL roll 882, 022534 and 023951). A concentrically fractured zone extends about one crater radius out from the crater edge; the surface beyond has a complex subradial texture. Several rimless craters in the smooth zone appear to be aligned along the arcuate fractures. Troughs composed of numerous coalescing craterlets and grooves extend to the north-northeast and south-southwest of the main crater. Small rimmed craters to the west may be impact craters unrelated to the regional structure. (d) South Spot viewed on Rev 32, 48 hours after the previous view (IPL roll 882, 033019 and 033901). The differences are due to real changes in the dust cloud or in the lighting and view paths through the dust. The disappearance of the radial facies on the northwestern rim suggests that other apparently smooth areas, such as the crater floor, actually may be concealed by atmospheric dust.

sphere above the high terrain if the dust is uniformly mixed. There is evidence for both hypotheses. The wide distribution of the surface obscuration and the apparent correlation between brightness and elevation, as well as the scale-height variation of the dust in limb frames, indicate thorough mixing of the dust. Regional nonuniformities in obscuration are indicated by the relative clarity of the south polar region, the complex structure of northern limbs, and perhaps by the clarity of Nix Olympica, which may contradict the altitude-clarity relationship. Radar data do not show this feature to be a particularly high object (*12*).

The height of features on the limb is not known because the limb of the solid planet cannot be seen. However, if the dust is well mixed we can infer a height. A well-mixed dust layer with τ value of 2 would not show a brightness decrease on the limb below heights at which the density is about 1/40 of the surface density. This implies that the lower part of the region of brightness decline is between 3 and 4 scale heights (30 to 40 km) above the surface. On this basis, the thin detached layer would be near 60 km, at a pressure between 0.1 and 0.01 mb. At least some of the wave clouds near the terminator may be occurring in this high layer. The nearest terrestrial analogs to a scattering layer in this pressure range are noctilucent clouds, which are sometimes apparent near or beyond the terminator during the summer at high latitudes.

Surface features of the south polar region. One objective of the Mariner 9 television experiment is to monitor the retreating south polar cap and to compare the exposed surface features with their frost-covered appearance recorded by Mariner 7 in 1969. These observations should provide evidence about the nature and origin of the features and terrains peculiar to the south polar region. The problems involve the past and present thickness of the CO_2 ice, the possible presence of other frozen volatiles, the control of the distribution and thickness of the frost by regional topography, and the geological processes associated with polar phenomena that may have uniquely modified that topography.

Owing partly to the high intrinsic contrast between the cap and the adjacent ground, it has been possible for Mariner 9 to monitor frost distribution throughout the dust storm. Correlation with the Mariner 7 pictures shows that the residual cap lies within the region of peculiar curvilinear features previously seen (*16*) near the south pole. Figure 7 shows the south polar cap as viewed by Mariner 7 late in the Martian southern winter and by Mariner 9 during the Martian southern summer. The planimetric similarity of the curvilinear patterns in both views is evident. However, in the 1969 picture the streaks are bright, being highlighted by frost, whereas they are dark in the Mariner 9 pictures. It is now evident that these curvilinear patterns are permanent topographic forms that control the outline of the residual cap as it retreats. It was observed in 1969 that local topography, principally craters, strongly controlled the detailed form of the margin of the retreating cap near 60°S latitude. Parts of the boundary and interior of the retreating cap, as seen in the Mariner 9 pictures, are remarkably regular and uniform and, therefore, appear to contain few craters. The topography seems to be limited primarily to curvilinear ridges or troughs, or both, perhaps of a highly subdued character.

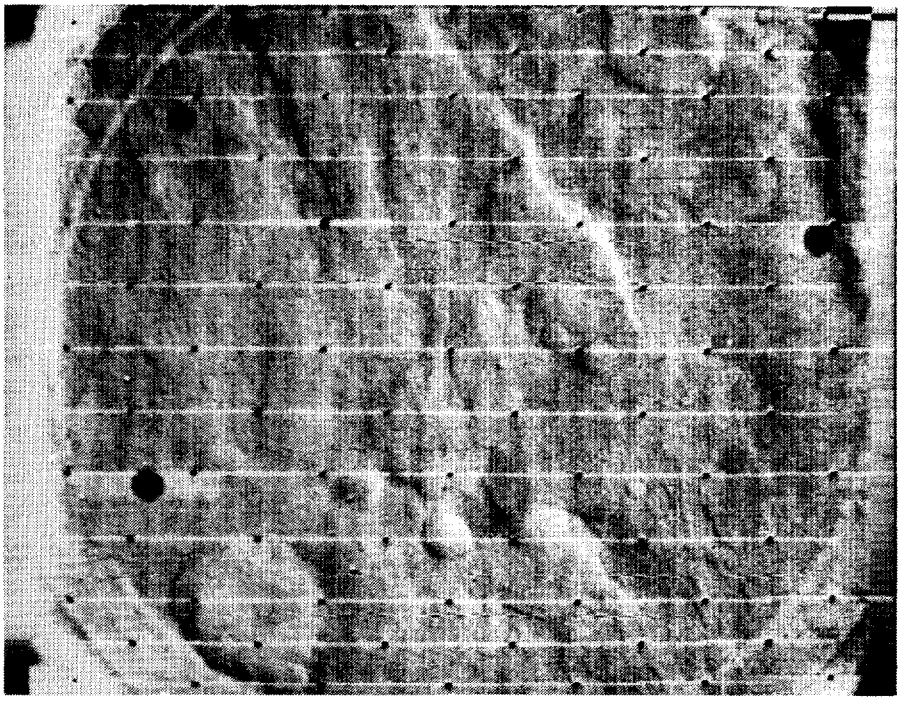

Fig. 11. Linear scarps, possibly a product of block faulting, west of Solis Lacus. As in almost all Mariner 9 pictures, the crater floors appear featureless. In this narrow-angle frame from Rev 42 the three dark circular spots are shadows of dust specks on the vidicon faceplate (JPL 4055-75).

Figure 8 presents selected high-resolution pictures that illustrate the variety of patterns displayed in the subliming cap. Whereas the low-resolution view gives the impression of a roughly circular pattern of conformal curvilinear features, the high-resolution images show a much more irregular pattern, although the individual dark streaks are quite uniform in width. One ring-shaped feature, probably a frost-free crater rim (see Fig. 8B), suggests that the positive relief may have defrosted there more rapidly than in adjacent areas. If this is true, the curvilinear streaks are most likely a complex of ridges in low relief. However, shallow scarps or troughs cannot be excluded by the available data.

The two wide-angle frames in Fig. 9 illustrate part of the significant disappearance of frost that occurred between Revs 11 and 44 (an interval of 16½ days). Two high-resolution views in the figure show details of the disappearance over 11½ days. As only a few centimeters of solid CO_2 could possibly sublime in this time, a very thin deposit covering a surface of extremely low relief is indicated in the areas that are clearing. It is still possible that thicker deposits exist elsewhere in the residual cap. The high-resolution frame acquired on Rev 34 suggests topograph-

ic control of the sublimation along small, shallow, irregular curvilinear features paralleling the main dark band.

At present, there is no way to determine whether the unusual topography at the site of the residual south polar cap is related to past or present thick ice deposits. Continued monitoring to record changes of detail combined with quantitative processing and manipulation of all the relevant photographic data may permit at least some intelligent speculations as to the history of this unique portion of the Martian surface.

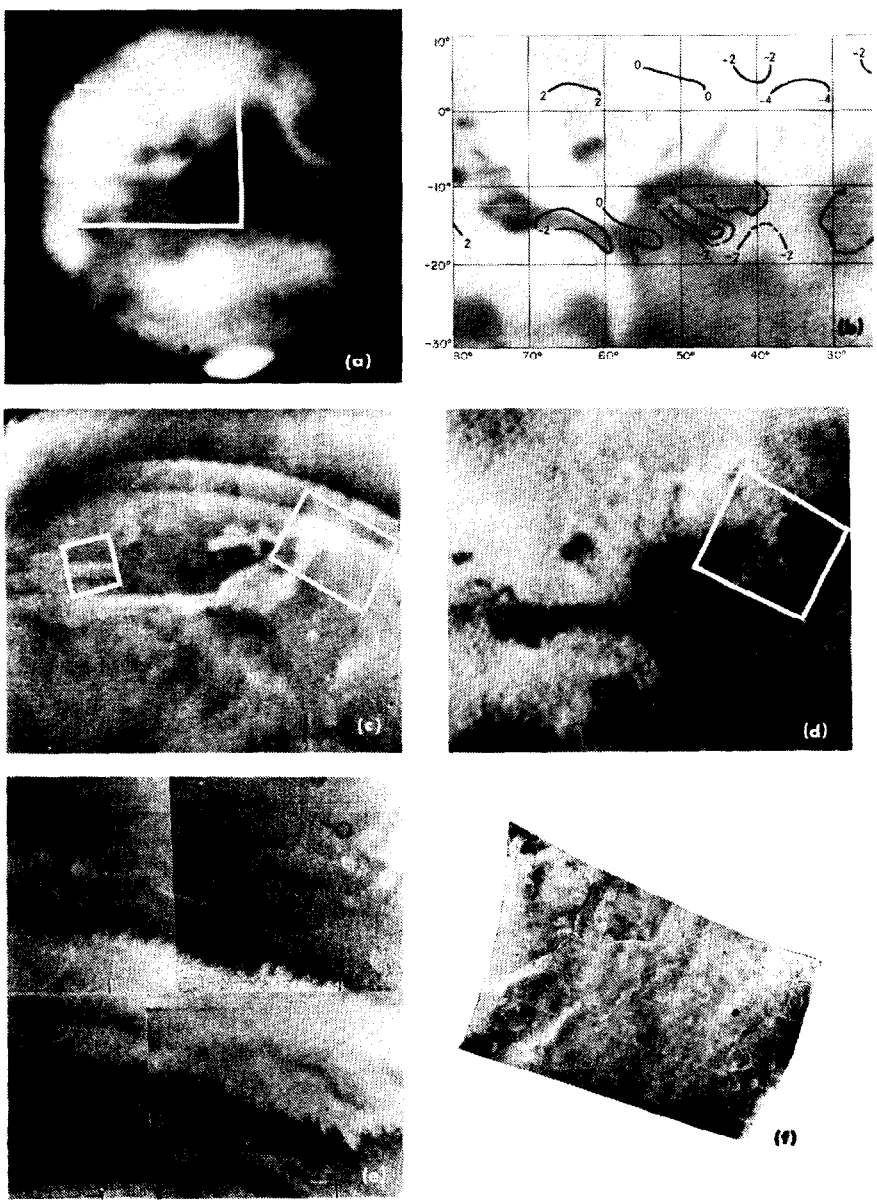

Fig. 12. Evidence of topographic control of atmospheric features. (a) The Aurorae Sinus region (center) displayed a discrete bright cloud during the 1956 dust storm. A similar discrete cloud appeared over Eos during the early stages of the 1971 dust storm (*1*). (b) Radar elevation contours (in kilometers) in the Eos region show that the brightest knot in the cloud lies near the deepest depression. The area shown corresponds with (c) and (d). (c) Eos-Ophir cloud complex as observed by Mariner 9 during POS 3 on 13 November 1971. The background is entirely obscured by atmospheric dust. The arcs are residual images of the limb from previous frames. The area shown corresponds to the area in the box in (a) (IPL roll 529, 252424). (d) Portion of a rectified Mariner 7 photomap of the same region as (c), with the normally visible dark markings. [From J. A. Cutts *et al.* (*13*)] (e) Narrow-angle mosaic of the western part of the cloud, photographed on 2 December. Some surface detail can be seen outside the sharp boundaries of the cloud. The area corresponds to that in the left-hand box in (c) (IPL roll 905; 201449, 202414, 203341, 204508). (f) Mariner 7 frame (6N7) showing the scarp-bounded valleys that delimit the eastern end of the cloud in the Eos region. These valleys contain the chaotic terrain discovered in 1969. The area shown corresponds to that in the right-hand box in (c) and the box in (d).

Geology. The atmosphere has been clear enough for geologic study of only a few areas, principally those indicated by radar and occultation data to be at high elevations, or those at far southern latitudes.

Perhaps the most significant pictures were taken in three of the four dark spots viewed in the preinsertion sequence. Nix Olympica, North Spot, and South Spot were photographed with narrow-angle frame tetrads; each contained a crater or a crater complex. The Nix Olympica (Fig. 10a) and North Spot (Fig. 10b) features are each composed of four or five intersecting craters that have floors at different elevations and appear to have formed successively. The visibility of the terrace edges indicates that the craters are not filled by dust; the apparent smoothness of the floors may be real, or the floors may be obscured by local dust. The craters are rimless or have very low rims; sharp ridges like those that surround most of the lunar craters are strikingly absent. On the highest-resolution photographs, those of South Spot, features less than 1 km in dimension can be distinguished (Fig. 10, c and d).

South Spot is a single, approximately circular structure, about 100 km across, that in its entirety is unlike any known terrestrial or lunar crater or any Martian crater observed on previous Mariner missions. The crater does resemble some large lunar craters in having a flat floor and completely terraced walls; it is distinctive in that a zone with a smooth surface broken into arcuate horsts and grabens concentric with the crater immediately surrounds the rim. Fresh, large lunar craters typically have coarse, hummocky topography immediately outside the crest of the rim that grades outward into radial ridges and grooves with low relief. Here the hummocky facies is absent, and a radial pattern is visible only beyond one crater radius from the edge of the crater. The elements in this zone are short and lobate, unlike the narrow, gradually tapering ridges radial to lunar craters. On the rim are several small (1 to 5 km in diameter) rimless craters, some of which appear to form arcuate chains. Major valleys extend to the northeast and southwest of the main crater (perhaps not coincidentally

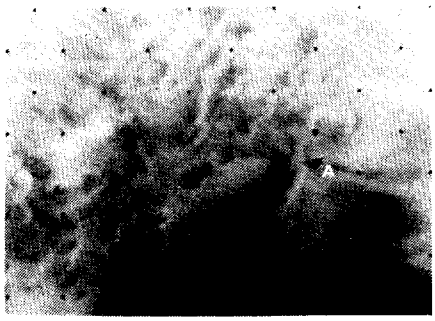

Fig. 13. Field of sinuous features near the south pole, in a wide-angle photograph from Rev 16 (JPL 4024-20). One feature apparently transects the rim of the crater *A*, which suggests that the features were formed by surficial processes.

in the direction of alignment of North Spot, Middle Spot, and South Spot). These valleys consist of many coalescing irregular craterlets and sinuous or linear grooves, and are another feature not closely matched in terrestrial or lunar craters.

The morphology of the craters in the three spots indicates subsidence. The most prominent features of large subsidence on the earth are volcanic calderas, which are caused by the withdrawal of magma, principally by eruption (*17*). Some calderas lie on the summits of broad volcanic shields, are accompanied by rimless pit craters on the upper flanks and lava flows on the lower slopes, and show multiple arcuate faults similar to those of South Spot, though rarely as well developed. The largest terrestrial calderas are irregular multiple structures with outlines and dimensions comparable to those of the Nix Olympica and North Spot features. A single, symmetrical caldera as large as the South Spot feature would be extraordinary on the Earth. An alternative hypothesis, that these craters are solely of impact origin, is difficult to reconcile with the absence of walls between component craters, the different levels of their floors in Nix Olympica and North Spot, and the lack of markedly elevated rims and hummocky rim deposits. Nevertheless, the continuing debate on the origin of many craters on the moon, where atmospheric processes neither cause surface modification nor degrade the viewing, indicates the advisability of caution in this preliminary interpretation, particularly since what we have seen may be only small parts of large structures. The fact that these features are elevated to a level of visibility when the rest of the planet is obscured suggests that they may not be typical of Mars as a whole. If the sharpness of the features and the smoothness of the surrounding terrain is not an effect of the conditions of viewing or image processing, these spots may be geologically young features compared to the heavily cratered areas observed in 1969 (*18*).

As the dust cleared elsewhere, some terrain became visible that exhibits more linear structural patterns than were recognized in the 1969 pictures. For example, west of Solis Lacus the surface is broken by irregular subparallel scarps (Fig. 11). The pattern is suggestive of block faulting on the earth; its true nature may become more apparent as broader areas become visible.

A pattern of light streaks in the region from Eos to Ophir, observed continuously since the POS sequences, is shown in Fig. 12. The brightest knot corresponds to a bright yellow cloud first viewed in photographs taken from the earth on 27 and 28 September, a few days after the 1971 dust storm began; a similar cloud was seen in the same location during the 1956 dust storm (Fig. 12a). Radar data show that in this region the dark areas (such as Aurorae Sinus) are high, while the bright regions are lower. The bright knot lies near a deep depression that is 6 km lower than the mean terrain (Fig. 12b; Fig. 4, point *F*). A comparison of the 1971 and 1969 Mariner pictures reveals that the bright markings obscure the dark markings that are normally visible in the region (Fig. 12, c and d) and suggests that the marking is an effect produced by a greater amount of dust in or above a system of valleys. It is not clear whether the cloud is a true concentration of dust or merely an apparent effect of in-

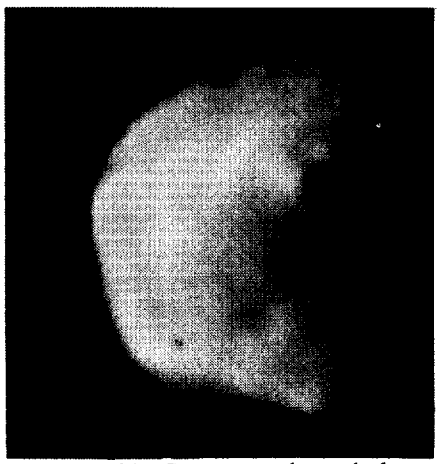

Fig. 14 (left). Computer-enhanced photograph of Deimos obtained on Rev 25 at a distance of 8830 km and a phase angle of 68° (IPL roll 752, 144007). Fig. 15 (right). Computer-enhanced frames of Phobos. (a) View obtained on Rev 31 at a distance of 14,440 km and a phase angle of 77° (IPL roll 792, 220312). (b) View obtained on Rev 34 at a distance of 5550 km and a phase angle of 56° (IPL roll 820, 002025).

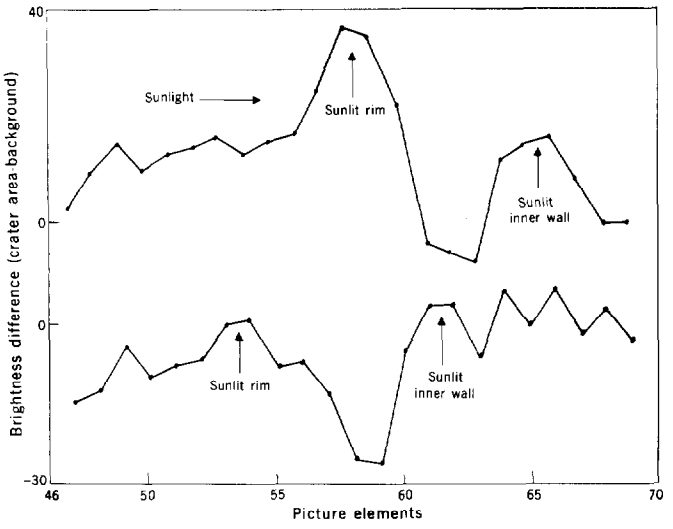

Fig. 16. Brightness traces across the two prominent craters on Deimos (see Fig. 14). From left to right, the trace progresses from near the sunlight limb to near the terminator. The ordinate is the difference in brightness between a trace across one of the craters and that across an uncratered part of Deimos. The image used to obtain the brightness values was not photometrically decalibrated.

creased path length through a more uniformly dust-laden atmosphere. Figure 12e is a narrow-angle tetrad in which part of the streak, and its scalloped, sharp boundaries, can be seen. Figure 12f shows that the eastern end of the cloud complex lies in the valley system containing the chaotic terrain discovered in 1969.

As in 1969, the south polar region presented features of types not seen in other southern latitudes. One of the more notable of these is a field of sinuous markings trending approximately north-south (Fig. 13). The identity of the pattern in views taken days apart shows that the markings are fixed features and not cloud or dust billows. One feature extends without deflection over what appears to be the rim of a crater, which suggests that the features have been produced by material transported over the surface with only slight control by underlying topography.

Satellite astronomy. Preorbital and orbital photographs of the Martian satellites, Phobos and Deimos, have provided new information about their orbits, shapes, sizes, albedos, and surface morphologies. To photograph Phobos and Deimos at close range it was necessary to obtain improved orbits. The first corrections to the orbital data were based on 21 pictures taken during the POS sequences that contain Phobos or Deimos together with stars. The ephemerides are being improved by incorporating pictures taken in orbit. A first-order analytic theory including zonal harmonics up to fourth order is used to model the motion of Phobos and Deimos (*19*). The initial conditions were obtained by fitting data obtained from Wilkins' theory (*20*). From the processed television data up to 28 November, the position of Deimos was determined with a standard deviation of 20 km. Since there were only five Phobos pictures, its position was obtained only to 100 km. Corrections to the mean orbital elements indicate that Phobos is approximately 2° ahead of its expected mean anomaly, while Deimos is about 1° behind. The inclinations of the orbital planes of Phobos and Deimos relative to the equatorial plane of the earth differ by 0.5° from those expected.

Figures 14 and 15 show the first closeup views ever obtained of these satellites. Both are irregular in shape, as expected for bodies too small for their gravitational fields to impose a spherical shape. The bottom side of Deimos displays an interesting indentation. Similarly, an indentation appears on the right side of Phobos in Fig. 15b. Phobos is estimated to be 25 ± 5 km long (east to west) and 21 ± 1 km wide (north to south); Deimos is 13.5 $\pm$ 2 km long and 12.0 ± 0.5 km wide. The nominal values are based upon the correction appropriate for a spherical object viewed at the observed phase angle. The larger limits of error for the length measurements reflect the uncertainty in allowing for the unilluminated portions of the body.

Combining the above dimensions with Kuiper's visual estimates from the earth of the magnitudes of the satellites (*6*), we infer a geometric albedo of 0.05 for both satellites, with a formal uncertainty of about 25 percent. Such a low albedo puts these two satellites among the darkest objects in the solar system, equivalent to the darkest parts of the lunar maria.

The picture of Deimos (Fig. 14) reveals two clear craterlike depressions near the terminator and a third dusky spot, which may be a crater. The craters are about 1.4 km in diameter, and their topography can be inferred from the patterns of brightness near and in the craters. Figure 16 shows a brightness profile through each crater in the direction from the limb to the terminator. The ordinate is a monotonic function of brightness but is not necessarily a linear function, since the pictures have not been photometrically decalibrated. To partially cancel the falloff of light toward the terminator, the data were normalized to the values on a parallel line across the smooth surface between the two craters. The shadowed, depressed interior for each crater is shown, and each crater is seen to have a bright outer rim on the terminator side. The presence of an outer rim is consistent with an impact origin for the craters. In the negligible gravity field of the satellites, little of the fragmental ejecta would settle near the crater, so that the rims correspond to the raised bedrock rims of terrestrial craters. These rims indicate some degree of plastic response. A more brittle response, which could depend upon the velocity of impact as well as the material of the satellite, would cause spalling of the outer shells of the satellite over a broad zone around the crater, around the antipodal point, and possibly even over the entire surface (*21*). While extensive spalling is not evident, some of the angular irregularities may have originated through such a process.

Many craters also appear on the pictures of Phobos. Particularly striking is the 5.3-km crater near the bottom (south pole) in Fig. 15a and near the center in Fig. 15b. The impact that produced this crater is close to the largest impact Phobos could have sustained without fracture and disruption.

Preliminary measurements indicate that the crater density on the two satellites is within about a factor of 3 of that corresponding to a surface saturated with craters. On the surface of Mars itself, the density of craters of similar size is roughly two orders of magnitude less. Thus, Phobos and Deimos serve as "control surfaces" for Mars and indicate that substantial erosive processes have acted to remove

ancient Martian craters. Phobos and Deimos can be regarded as old, relative to Martian surface structures on the kilometer scale.

HAROLD MASURSKY, R. M. BATSON
J. F. MCCAULEY, L. A. SODERBLOM
R. L. WILDEY
U.S. Geological Survey,
601 East Cedar Avenue,
Flagstaff, Arizona 86001

M. H. CARR, D. J. MILTON
D. E. WILHELMS
U.S. Geological Survey,
354 Middlefield Road,
Menlo Park, California 94025

B. A. SMITH, T. B. KIRBY
J. C. ROBINSON
Department of Astronomy,
New Mexico State University,
Las Cruces 88001

C. B. LEOVY
Department of Atmospheric Sciences,
University of Washington,
Seattle 98105

G. A. BRIGGS, T. C. DUXBURY
C. H. ACTON, JR.
Jet Propulsion Laboratory,
California Institute of Technology,
Pasadena 91103

B. C. MURRAY, J. A. CUTTS
R. P. SHARP, SUSAN SMITH
Division of Geological and Planetary Sciences, California Institute of Technology, Pasadena 91109

R. B. LEIGHTON
Division of Physics, Mathematics, and Astronomy, California Institute of Technology

C. SAGAN, J. VEVERKA, M. NOLAND
Laboratory for Planetary Studies,
Cornell University,
Ithaca, New York 14850

J. LEDERBERG, E. LEVINTHAL
Department of Genetics, Stanford University School of Medicine,
Stanford, California 94305

J. B. POLLACK, J. T. MOORE, JR.
Space Sciences Division,
Ames Research Center,
Moffett Field, California 94305

W. K. HARTMANN
IIT Research Institute, 60 West Giaconda Way, Tucson, Arizona 85704

E. N. SHIPLEY
Bellcomm, Inc.,
955 L'Enfant Plaza North, SW
Washington, D.C. 20024

G. DE VAUCOULEURS
Department of Astronomy, University of Texas, Austin 78712

M. E. DAVIES
Rand Corporation, 1700 Main Street, Santa Monica, California 90401

References and Notes

1. T. B. Kirby and J. C. Robinson, *Sky Telesc.* **42**, 264 (1971).
2. E. Pettit and R. S. Richardson, *Publ. Astron. Soc. Pac.* **67**, 62 (1955).
3. H. Masursky, R. Batson, W. Borgeson, M. Carr, J. McCauley, D. Milton, R. Wildey, D. Wilhelms, B. Murray, N. Horowitz, R. Leighton, R. Sharp, W. Thompson, G. Briggs, P. Chandeysson, E. Shipley, C. Sagan, J. Pollack, J. Lederberg, E. Levinthal, W. Hartmann, T. McCord, B. Smith, M. Davies, G. de Vaucouleurs, C. Leovy, *Icarus* **12**, 10 (1970).
4. A. A. Mikhailov, in *The Moon*, Z. Kopal and Z. K. Mikhailov, Eds. (Academic Press, New York, 1962), p. 3. Our "stretched" pictures correspond to the Russians' "photometric cross-sections."
5. A. T. Young, *Icarus* **11**, 1 (1969). The darkening parameter k is defined in terms of the brightness B, incidence angle i, and emission angle ϵ by $B = B_0(\cos i)^k(\cos \epsilon)^{k-1}$, in which the parameters B_0 and k are both functions of phase angle in general.
6. D. L. Harris, in *Planets and Satellites*, G. P. Kuiper and B. M. Middlehurst, Eds. (Univ. of Chicago Press, Chicago, 1961), p. 289.
7. E.-M. Antoniadi, *La Planete Mars 1659–1929* (Librairie Scientifique Hermann, Paris, 1930).
8. Contrast is defined here as the difference in brightness of the dark and light areas divided by the brightness of the dark area.
9. Optical depth is the natural logarithm of the reciprocal of the atmospheric transmission factor. Extinction is the sum of attenuation caused by scattering and by absorption.
10. D. J. Van Blerkom, *Icarus* **14**, 235 (1971).
11. This is based on an average of 90 percent for Mariner 7 red and green photographs at a different season but with similar illumination and on a measurement of 60 percent in a Lowell Observatory plate at the same season and illumination. The latter value is expected to be somewhat below the true value because of the small cap size in the image.
12. G. H. Pettengill, C. C. Counselman, L. P. Rainville, I. I. Shapiro, *Astron. J.* **74**, 461 (1969); A. E. E. Rogers, M. E. Ash, C. C. Counselman, I. I. Shapiro, G. H. Pettengill, *Radio Sci.* **5**, 465 (1970); R. M. Goldstein, W. G. Melbourne, G. A. Morris, G. S. Downs, D. A. O'Handley, *ibid.*, p. 475; G. H. Pettengill, A. E. E. Rogers, I. I. Shapiro, *Science* **174**, 1321 (1971); G. S. Downs, R. M. Goldstein, R. R. Green, G. A. Morris, *ibid.*, p. 1324.
13. J. A. Cutts, L. A. Soderblom, R. P. Sharp, B. A. Smith, B. C. Murray, *J. Geophys. Res.* **76**, 343 (1971).
14. C. Sagan and J. B. Pollack, *Nature* **223**, 791 (1969).
15. C. Sagan, J. Veverka, P. Gierasch, *Icarus* **15**, 253 (1971); P. Gierasch and C. Sagan, *ibid.* **14**, 312 (1971).
16. R. P. Sharp, B. C. Murray, R. B. Leighton, L. A. Soderblom, J. A. Cutts, *J. Geophys. Res.* **76**, 357 (1971).
17. H. Williams, *Univ. Calif. Publ. Geol. Sci.* **25**, 239 (1941).
18. B. C. Murray, L. A. Soderblom, R. P. Sharp, J. A. Cutts, *J. Geophys. Res.* **71**, 313 (1966).
19. K. Aksnes, paper presented at the 8th annual seminar on Problems in Celestial Mechanics, University of Texas, Austin, 1970.
20. G. A. Wilkins, in *Mantles of the Earth and Terrestrial Planets, NATO Advanced Study Institute, University of Newcastle-upon-Tyne, 1966* (Interscience, London, 1967), p. 77.
21. D. E. Gault and J. A. Wedekind, *J. Geophys. Res.* **74**, 6780 (1969).
22. E. C. Slipher, *The Photographic Story of Mars* (Northland Press, Flagstaff, Ariz. 1962), p. 142.
23. We thank E. M. Shoemaker and A. P. Ingersoll for reviewing the manuscript. We also thank R. Tyner and S. Reed for making mosaics of the pictures during mission operations. This work was performed for the Jet Propulsion Laboratory, California Institute of Technology, under NASA contract NAS 7-100.

27 December 1971